Differential expression of outer hair cell potassium currents in the isolated cochlea of the guinea-pig

F. Mammano and J. F. Ashmore*

Department of Physiology, School of Medical Sciences, University Walk, Bristol BS8 1TD, UK

1. Whole-cell currents were recorded from outer hair cells (OHCs) in undissociated tissues from the organ of Corti. The experiments allowed ionic currents to be measured in cells with precise localization on the three most apical cochlear turns.

2. Two major potassium currents were expressed in the cells. One current, named I_K, was half-activated at −24 mV and was most prominent in the most apical turn, turn 4. A second, named $I_{K,n}$, was half-activated at −92 mV and was the major contributor to the current–voltage (I–V) curve of cells from the more basal turns, turns 3 and 2, of the cochlea.

3. I_K was specifically blocked by 100 μM 4-aminopyridine (4-AP). In contrast, $I_{K,n}$ was reduced by 5 mM external barium. Superfusion with zero calcium produced no effect on currents in the range from −60 to 0 mV, but reduced currents by a maximum of 15% outside this range.

4. The cell input conductance increased systematically from 3·4 nS in turn 4 to 40 nS in turn 2 measured at a holding potential of −70 mV.

5. The mean leak conductance, measured from the slope of the I–V curve at −110 mV, decreased systematically from 5·2 nS in turn 2, to 2·9 nS in turn 3 and 2·2 nS in turn 4.

6. These data show that hair cell properties can be determined in undissociated cells and are likely to provide a good estimate of the properties of the cells in the intact cochlea. Differences with the properties of isolated OHCs are discussed.

The physical basis of the frequency–place map found in the mammalian cochlea is known to depend primarily upon the longitudinal stiffness gradient of the basilar membrane. In addition to this macroscopic gradient, systematic variations in the cochlear partition have been emphasized for the cellular constituents of the organ of Corti (Vôldrich, 1983). There are systematic variations of cell dimension (Pujol, Lenoir, Ladrech, Tribillac & Rebillard, 1992), density of efferent innervation (Spoendlin, 1978), density of purinergic receptors (Housley, Connor & Raybould, 1995) and the input conductance of the isolated outer hair cells (OHCs) (Housley & Ashmore, 1992). Such electrical differences are known to be critical in non-mammalian species where the electrical filtering properties and the expression of ionic conductances of the cells vary systematically along the auditory structures (Art & Fettiplace, 1987; Murrow, 1994). However, electrical tuning is not employed in the mammalian cochlea and such physiological variations may play a different role.

As has been appreciated before, ambiguities arise when trying to determine cochlear origin of isolated cells from length measurements alone because equally long OHCs, particularly in the 30–55 μm range, may belong either to cochlear turn 4 row 1 or turn 2 row 3 (Pujol *et al.* 1992; Housley & Ashmore, 1992). We describe here results from patch clamped cells in the organ of Corti from the isolated temporal bone where the position of the cells along the length of the basilar membrane and within each row can be determined unambiguously (Mammano & Ashmore, 1993; Mammano, Kros & Ashmore, 1995). It will be shown that two currents are present in these cells which can be distinguished pharmacologically and we describe the differential expression of these currents in different turns. The differences with isolated cells will be indicated.

A preliminary report of this work has been presented to The Physiological Society (Mammano & Ashmore, 1995).

METHODS

Tissue preparation

Adult albino guinea-pigs (250–400 g) were killed by rapid cervical dislocation. After dissecting the temporal bone, the bulla was

* To whom correspondence should be addressed at the Department of Physiology, University College London, Gower Street, London WC1E 6BT, UK.

opened and firmly held by attaching the bone with dental acrylic to a Perspex chamber perfused with oxygenated phosphate buffer solution (PBS). The organ of Corti in turn 4 was observed under low magnification from scala media by gently scraping away the bony wall of the cochlea. Access to turns 3 and 2 was obtained by removing the overlying turns. In general recording conditions were more stable from the more apical turns and this is reflected in the larger data sets for turns 4 and 3. In each case Reissner's membrane was carefully peeled off leaving the partition intact. Cells in the partition were illuminated by a 1 mm fibre optic light guide gently pushed perpendicularly against the outside of the cochlear wall and viewed using a ×40, 0·75 NA water-immersion objective (Zeiss, Germany). With suitable positioning of the light guide, a clear view of the cell boundaries was possible to allow positioning of the patch pipette. Experiments were conducted at a temperature of 24–28 °C.

Solutions

All solution changes within the bath could be made within 1 min. The external solution (phosphate-buffered saline (PBS)) contained (mM): NaCl, 142; KCl, 4·0; $CaCl_2$, 1·0; $MgCl_2$, 2·0; Na_2HPO_4, 8·0; NaH_2PO_4, 2·0; pH was adjusted to 7·3 with NaOH and osmolarity to 325 ± 2 mosmol l^{-1} with D-glucose. When testing the effect of 5 mM Ba^{2+}, cells were initially bathed in PBS containing 1 mM $CaCl_2$ and 4 mM $MgCl_2$ and then washed through for 2–3 min with an otherwise identical isosmotic solution where 5 mM Hepes was substituted for the phosphates. Hepes solution with 5 mM $BaCl_2$ and no other divalent cations was then applied for up to 15 min, followed by return to PBS. Control experiments to assess the effects of Mg^{2+} were performed in PBS with up to 10 mM $MgCl_2$ and 1 mM $CaCl_2$. There were no appreciable differences in the recorded currents. Nominal zero calcium buffers were PBS with 3 mM $MgCl_2$, without calcium-chelating agents and no added $CaCl_2$. Tetraethylammonium (TEA) was used as the chloride and TEACl (30 mM) replaced an equal concentration of NaCl in PBS. Drugs applied in the micromolar concentration range (4-aminopyridine (4-AP)) were simply added to normal PBS. All drugs were obtained from Sigma.

Data acquisition

Pipettes were pulled on a two-stage vertical puller (PP-83, Narishige, Tokyo, Japan) from 1·5 mm o.d. soda glass (Clark Electromedical, Pangbourne, UK). They were filled with a solution containing (mM): KCl, 144; $MgCl_2$, 2·0; EGTA, 5·0; Na_2HPO_4, 8·0; NaH_2PO_4, 2·0; the solution was adjusted to pH 7·2 with KOH and brought to 325 mosmol l^{-1} with D-glucose. Recordings were made using an EPC/7 amplifier (List Medical). The pipette resistance was typically 3 MΩ when measured in the bath. The mean (uncompensated) access resistance in the thirty-eight cells reported, measured upon achieving the whole-cell configuration, was 10 MΩ (range 7–18 MΩ). Current and voltage were sampled at either 2·5 or 25 kHz using a standard laboratory interface (CED 1401plus, Cambridge Electronic Design, Cambridge, UK) under control of software written for the purpose. Potentials were corrected for measured liquid junction potentials (typically −4 mV).

Curve fitting was carried out using routines for Matlab 4·0 (The Mathworks, Natick, MA, USA) based on library function FMINS that minimizes a function of several variables using the Nelder–Mead simplex search algorithm. This is a direct search method that does not require gradient or other derivative information (e.g. Dennis & Woods, 1987) and thus is better suited to relatively noisy data.

Statistical data results are expressed as means ± S.D.

RESULTS

Whole-cell outer hair cell currents

Under direct visual control, patch pipettes were carefully advanced through the thin layer of Hensen's cells near the tectorial membrane border. Whole-cell tight-seal recordings were made from the third row of OHCs adjacent to the Hensen's cells. Cells reported here were located in the cochlear turn 2 (at the site tuned to approximately 7 kHz), in turn 3 (2 kHz) and in turn 4 (0·5 kHz) (Greenwood, 1990; Pujol *et al.* 1992).

On patch rupture the pipette recorded a zero current potential of −30 to −40 mV, which rapidly became more negative as the pipette contents equilibrated with the cell interior over 30–60 s. After stabilization, the mean zero-current potential recorded under whole-cell conditions was close to the value of −70 mV found *in vivo* using microelectrodes (Dallos, 1985). There was no statistically significant difference between the zero-current potentials (Table 1, column 3) recorded in these three turns. Cells were held close to this stable zero-current potential and for the purpose of comparison were compared at −70 mV.

Typical voltage and current records obtained from cells in the three turns are shown in Fig. 1. Hyperpolarizing steps elicited large inward currents in turn 2 which decayed with a variable time constant (10–30 ms) depending on membrane potential (Fig. 1*A*). The size of the inward currents decreased considerably from turn 2 (where they were prominent) to turn 4 (where they were almost absent). In turn 2, depolarizing commands produced outward currents which reached a maximum in 10–20 ms and did not decay appreciably during the 100 ms voltage steps. In turn 3 and turn 4, the total outward current elicited by comparable commands also peaked and then partially decayed, but with time constants which were voltage dependent, with a value of approximately 350 ms near −20 mV to 125 ms near +30 mV. The maximum currents at the end of the 100 ms step were 1·4 times larger in turn 2 than in turn 3 and 1·8 times larger than in turn 4.

In addition to these outward currents, a fast transient current, which lasted 1–2 ms and could not be compensated by the amplifier circuitry, was also present at onset and offset of the command step. The amplitude of the transient was a function of the step size and cell location in the cochlea, the smaller cells in the more basal region producing proportionally smaller transients for the same applied potential. This current can be identified as a voltage-dependent component of the cell capacitance (Ashmore, 1989; Santos-Sacchi, 1991) and is associated with OHC length changes seen in this preparation (Mammano *et al.* 1995).

The steady-state current–voltage relation (I–V) was measured at the end of each 100 ms command step (Fig. 1*B*). The maximum slope conductance in turn 2 was comparable to that in turn 3 and 16% larger than in turn 4,

Table 1. Properties of outer hair cells from turns 2–4

Turn	n	V_z (mV)	C_m (pF)	R_{in} (MΩ)	g_L (nS)	γ_{max} (nS)	i_{max} (nA)	C_1 (nS)	C_2 (nS)	ρ (C_1/C_2)
2	5	−75 ± 4	13·3 ± 2·0	25 ± 2	5·2 ± 0·7	50·6 ± 9·7	2·7 ± 0·1	30 ± 2	0·6 ± 0·1	53 ± 13
3	19	−76 ± 4	30·1 ± 2·9	100 ± 30	2·9 ± 1·6	48·6 ± 22·4	1·9 ± 0·5	10 ± 4	10 ± 5	1·1 ± 0·5
4	14	−70 ± 5	37·5 ± 3·1	294 ± 70	2·2 ± 0·7	43·9 ± 13·9	1·5 ± 0·4	2 ± 0·6	14 ± 5	0·17 ± 0·08

Input capacitance, C_m, and resistance, R_{in}, were measured at −70 mV, close to the observed zero current potential, V_z. The residual slope conductance, g_L (column 6), was measured at −120 mV. Maximum current, i_{max} (column 8), was measured at 0 mV. The maximum slope conductance, γ_{max} (column 7), was measured at more positive potentials towards the cochlear apex: at −54 mV (turn 2), at −21 mV (turn 3) and at −14 mV (turn 4) reflecting the increasing contribution of I_K. Mean values of the parameters C_1 and C_2 as defined in eqn (3).

but in turn 2 it was reached at potentials 30 mV more hyperpolarized than in both turns 3 and 4. A noticeable feature of the records, compared with those published for isolated cells, was the relatively small slope of the I–V curve at potentials negative to −110 mV (Housley & Ashmore, 1992). This residual current was not subtracted from any of the records shown in the figures.

Table 1 presents mean data for all fourteen cells recorded from turn 4, nineteen cells from turn 3 and five cells from

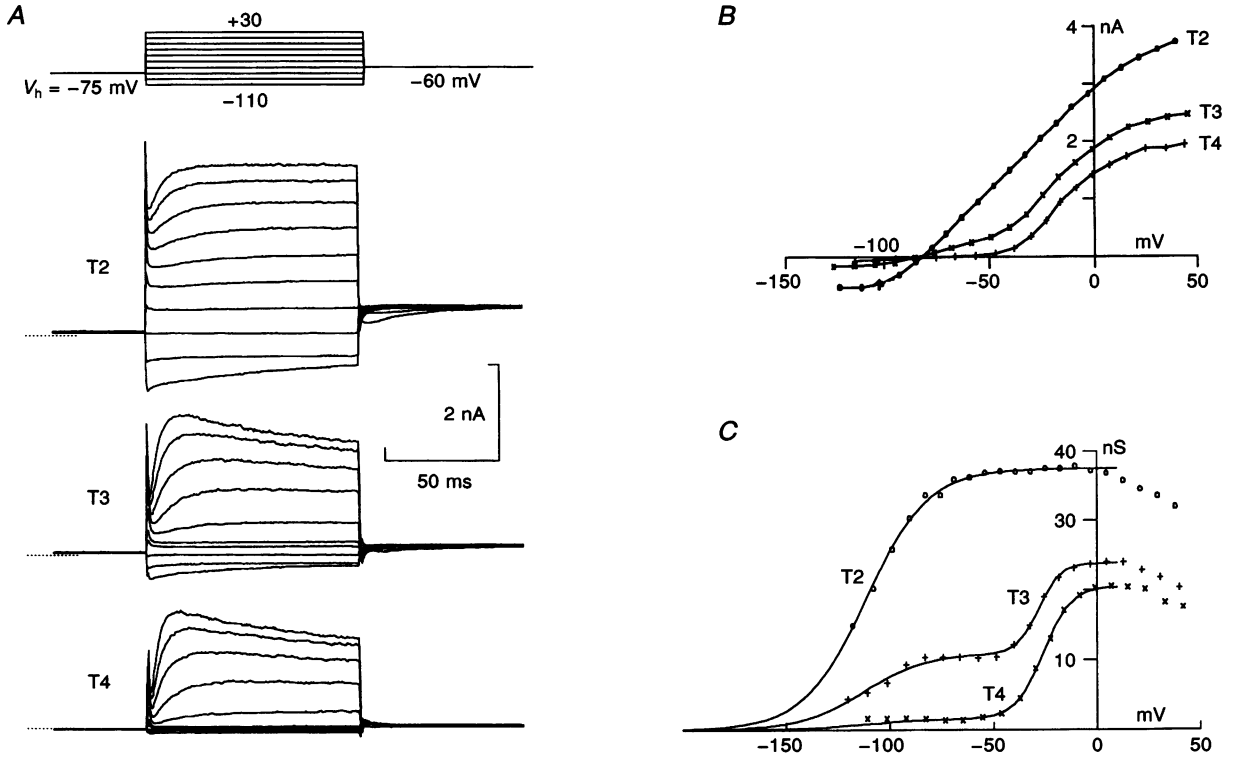

Figure 1. Whole-cell currents in the intact adult organ of Corti third row outer hair cells

A: top, applied voltage commands, corrected for series resistance; T2–T4, currents in turn 2 (near the 7 kHz site), turn 3 (2 kHz) and turn 4 (0·5 kHz), respectively. The dotted line in this and subsequent figures shows position of zero current. Data sampled at 2·5 kHz. V_h represents the holding potential. *B*, I–V relations obtained from current and voltage values in *A*. Data measured 5 ms before command offset. *C*, chord conductance for cells shown in *B*, computed from the estimated reversal potential: $V_R = -92$ mV. Continuous lines are each a linear combination of two Boltzmann functions (as in eqn (1)) with different scaling coefficients. The fits to the data are (C_1, C_2): turn 2, 37·5, 0·75 nS; turn 3, 11·0, 13·3 nS; and turn 4, 1·68, 18·4 nS. $g(V)$ was fitted to the data in the range from −120 to 0 mV and extrapolated to more negative potentials.

turn 2. The table shows that the membrane capacitance (column 4) increased by 3 times between turn 2 and turn 4 as the cells increased in length. The input resistance (column 5), measured at −70 mV, also increased as cells were taken from progressively more apical sites. The input resistance thus varied more than tenfold for the cells measured, from 24·4 MΩ in turn 2 to 294 MΩ in turn 4. However, the maximum measured slope conductance (50·6 nS in turn 2 and 43·9 nS in turn 4) did not show the same degree of variation. The observation is consistent with the presence of substantial potassium current activated at −70 mV in the more basal cells.

Two potassium currents

Figure 1*C* shows that at least two currents with different activation ranges were present in the cells. The conductance–voltage relations were derived from the *I–V* curves by assuming that the current, $I(V)$, was given by:

$$I(V) = G(V)(V - V_R) + g_L V, \quad (1)$$

where $G(V)$ is a voltage-dependent conductance and g_L, a leak conductance for a non-selective channel. The voltage-dependent currents were taken to be potassium currents as will be described below. The value of the reversal potential (V_R) of −92 mV used in eqn (1) was taken as the fixed potassium equilibrium potential based on the Nernst equation for the given experimental solutions. This choice of V_R stabilized the fitting algorithm. The resulting computed g_L was in good agreement with the slope of the *I–V* curve negative to −110 mV (Table 1, column 6). To provide a fit, $G(V)$ was taken to be a linear combination of two conductances, g_1 and g_2:

$$G(V) = g_1(V) + g_2(V), \quad (2)$$

where each function g_i was assumed to be a Boltzmann form:

$$g_1(V) = C_1[1 + \exp(-[V - V_1]/(\alpha_1)]^{-1},$$
$$g_2(V) = C_2[1 + \exp(-[V - V_2]/(\alpha_2)]^{-1}. \quad (3)$$

Different scaling coefficients, C_1 and C_2 (the maximum conductances for g_1 and g_2), were necessary for turn 2, 3 and 4 data. C_1 and C_2 were determined as the coefficients of a general least-squares procedure taking g_1/C_1 and g_2/C_2 as basis functions (Press, Flannery, Teukolsky & Vetterling, 1988). However, above 0 mV the slope of the *I–V* curve (Fig. 1*B*) became negative, probably due to the calcium dependence of the current. In these cases, the data were only fitted up to 0 mV as the simple representation given in eqn (3) no longer holds.

The two components of the voltage-dependent conductance exhibited comparable degrees of expression in turn 3. Thus, the exponential parameters of g_1 and g_2 were selected as mean values from turn 3 records ($n = 19$). The first component of conductance in eqn (3), associated with g_1, was half-activated at $V_1 = -92 \pm 15$ mV with a reciprocal slope $\alpha_1 = -17 \pm 8$ mV. Being largely activated at rest (−70 mV), it would thus contribute to maintaining the zero-current potential at hyperpolarized values. It deactivated upon hyperpolarization (Fig. 1*A*) and was identified as $I_{K,n}$,

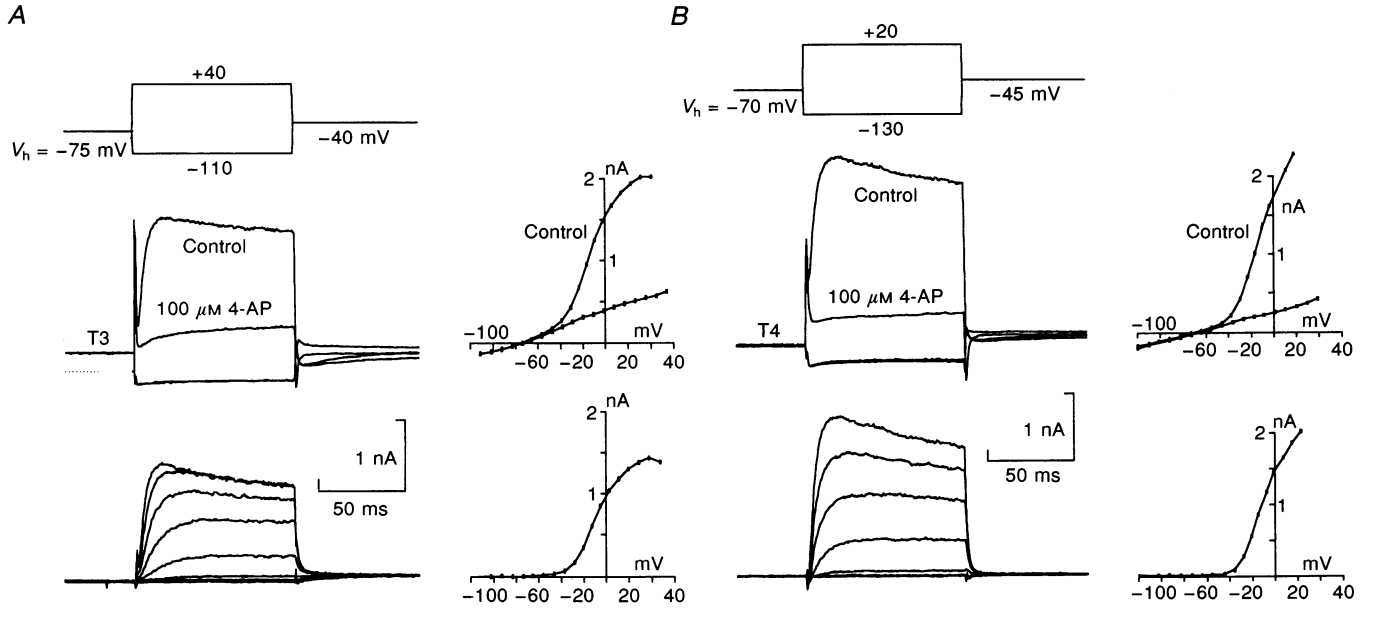

Figure 2. Effect of 4-AP on OHC currents

A, turn 3 OHC currents (T3) with and without 100 μM external 4-AP. Voltage command shown above; series resistance corrected. Bottom left panel shows 4-AP-sensitive current, I_K, obtained by subtraction at eight 10 mV holding steps starting from −35 mV. Right panel: top, *I–V* curve with and without 4-AP; bottom, *I–V* curve of 4-AP-sensitive current. *B*, same as *A* for turn 4 currents (T4). In both turns the outward current activating above −40 mV was completely blocked whereas inward currents and zero-current potential were unaffected.

previously described in isolated OHCs (Housley & Ashmore, 1992). The second component, associated with g_2, represents the conductance found for many outward rectifiers, with a half-activation at $V_2 = -24 \pm 5$ mV and a reciprocal slope $\alpha_2 = -6{\cdot}4 \pm 1{\cdot}0$ mV. It will be labelled as I_K. Being half-activated at relatively depolarized levels this current was responsible for the increase in the slope of turn 3 and turn 4 I–V relations between −40 and 0 mV.

The ratio $\rho = C_1/C_2$, representing the relative contribution $I_{K,n} : I_K$, was in excess of 50 in turn 2, approximately 1 in turn 3 and smaller than 0·2 in turn 4 (Table 1, last column). Thus the current in the short basal cells was dominated by $I_{K,n}$ whereas those of the long apical cells were almost entirely due to I_K. Cells in the middle region exhibited about equal ratios of currents ($\rho = 1{\cdot}1$). The gradual alteration in the balance between the two currents produced a shift of the potential at which the maximum slope conductance was measured. The maximum slope conductance was found at more depolarized values on progressing from base to apex (Table 1, column 7).

To demonstrate that these currents were carried by K^+, the tail currents were measured on stepping to a negative potential after a constant depolarizing step to −24 mV. The tail currents reversed at −79 mV (turn 4), −82 mV (turn 3) and −85 mV (turn 2). (An example of the data for turn 4 is reported in Mammano *et al.* 1995, Fig. 2*B*.) As the expected value for the reversal potential for K^+ was −92 mV, the data are consistent with the assumption that the currents were carried by potassium ions.

Pharmacological separation of the OHC currents

The two K^+ currents could be distinguished pharmacologically. These experiments were carried out in turn 4 and turn 3 cells only as recordings could be obtained from them often for more than 35 min. I_K was reversibly and selectively suppressed by 100 μM 4-AP when applied externally (Fig. 2). The effect of 4-AP was to suppress outward currents by 68 ± 7% near 0 mV in turn 3 ($n = 3$), by 85 ± 6% in turn 4 ($n = 3$) and to remove prominent deactivation of the current. 4-AP did not affect $I_{K,n}$, as judged from the insensitivity of the inward current and the zero-current potentials.

Figure 2*A* shows a turn 3 cell and Fig. 2*B* a turn 4 cell when 4-AP was superfused around the preparation. The figure shows the records obtained by subtracting currents in 4-AP + PBS from those in controls and represent the 4-AP-sensitive current I_K. The data show that turn 4 cells exhibit a larger fraction of I_K.

Although $I_{K,n}$ was insensitive to 4-AP, it was reversibly reduced by 5 mM external Ba^{2+} (Fig. 3). The effect of Ba^{2+} was to produce a shift in the zero-current potential by about 10 mV in the depolarized direction in turn 3 (Fig. 3*A*) and up to 20 mV in turn 4 (Fig. 3*B*). Currents activated by depolarization were also reduced, by 64 ± 10% at 0 mV in turn 3 ($n = 3$) and 35 ± 8% in turn 4 ($n = 3$). Although the

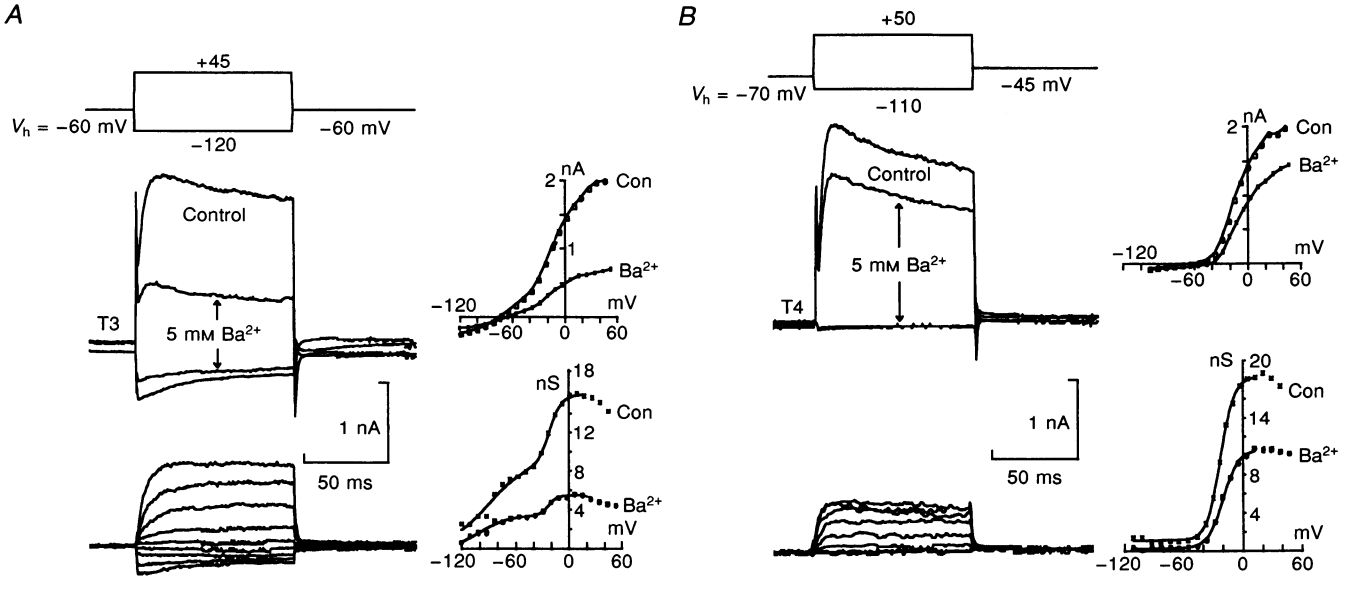

Figure 3. Effect of barium on OHC currents

A, turn 3 currents (T3) obtained with and without 5 mM external Ba^{2+}. Voltage command timing shown above. Right, I–V curves for data in left panel (Con, control; Ba^{2+}, in the presence of Ba^{2+}). Bottom left, current fraction sensitive to Ba^{2+}, obtained by subtraction of responses in 5 mM Ba^{2+} from controls, nine 15 mV steps starting from −90 mV. The voltage steps had the same timing as above. Bottom right, chord conductance for I–V series to the left, computed from the estimated reversal potential: $V_R = -92$ mV. Continuous lines are fits to the data using eqn (1) (labelled Con and Ba^{2+} as for I–V curves). *B*, same as *A* for turn 4 currents (T4). In both turns the inward currents were decreased and zero current shifted to more depolarized values.

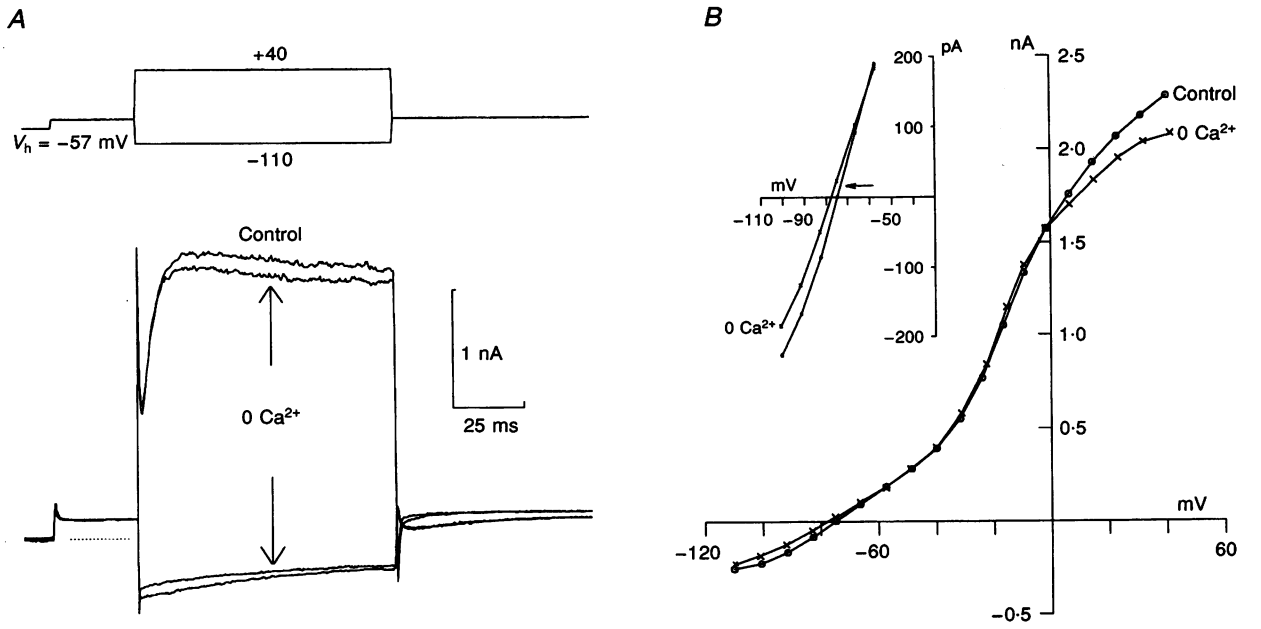

Figure 4. Effect of superfusion with nominally zero calcium on OHC currents

A, zero calcium reduced both outward and inward currents particularly above 0 mV. *B*, steady-state *I–V* curve of data in *A*. Inset: *I–V* curve expanded to show 3 mV hyperpolarizing shift of zero current (horizontal arrow) in zero $[Ca^{2+}]_o$. Cell location, turn 3.

effects of barium on $I_{K,n}$ have been reported (Nakagawa, Kakehata, Yamamoto, Akaike, Komune & Uemura, 1994), the data here, which cover a full range of potentials, show that the effect is not completely selective, as the barium-sensitive current has an *I–V* curve (in both turn 4 and turn 3) which is not identical to that predicted from the form of $g_1(V)$ (eqn (2)). The shift was less than expected for a complete blockage of $I_{K,n}$, indicating that Ba^{2+} is only partially effective at these concentrations. Therefore the currents obtained by subtraction should not be regarded as representative of $I_{K,n}$ alone. Nevertheless, the simplest explanation of the data as to why Ba^{2+} affected turn 3 cells more than turn 4 cells is that $I_{K,n}$ is expressed more in turn 3 and the effects of Ba^{2+} involve a direct action on the potassium channels themselves.

The effect of TEA as a conventional blocker of potassium currents was also investigated. TEA (30 mM) reduced the total outward current at 0 mV by about 30 ± 5% in turn 3 ($n = 2$) and 23 ± 4% in turn 4 ($n = 2$). The action was less specific than 4-AP. TEA also shifted the zero-current potential by about 3 mV in turn 3 and 6 mV in turn 4 in the depolarizing direction in the four cells studied.

Figure 4 shows the effect of removing external calcium. Nominally zero calcium reduced inward current at −110 mV by 12 ± 8% ($n = 3$) as well as reducing outward current above 0 mV. Together with the decline of the chord conductance at positive potentials (Fig. 1*C*), this provides evidence of a partial calcium dependence of both currents, $I_{K,n}$ and I_K. However, the conductance in the range from −35 to 0 mV, where the activation of I_K is steepest, was substantially unchanged. A potassium conductance, activated above −35 mV, has been identified in isolated OHCs (Housley & Ashmore, 1992) and it was anticipated that this current was associated with maxi-K channels, which should be calcium dependent. It was noted that, when cells were stepped to −130 mV for 30 ms before the *I–V* commands, the cell conductance near 0 mV increased by 5% (data not shown). One possible explanation for both of these

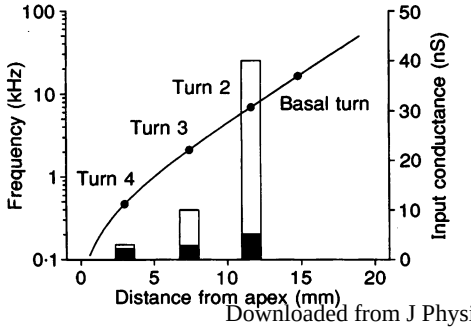

Figure 5. Frequency–place map for guinea-pig OHC input conductance

Abscissa: distance, x, along the cochlea with recording positions marked. Basal turn also indicated for completeness. The corresponding best frequency, f, is drawn as a continuous line according to:

$$f = 0{\cdot}35(10^{(2{\cdot}1x/18{\cdot}5)} - 0{\cdot}85)$$

(Greenwood, 1990). The input conductances (axis scale to the right) at −70 mV (Table 1, column 5) have been drawn as open bars; the filled bars, superimposed, are the leak conductances, g_L. See text.

findings is that calcium does enter the cell with hyperpolarizing steps, but that in this preparation intracellular calcium is strongly buffered.

Figure 4*B* shows that near −70 mV, close to the zero-current potential of the cells and where the current was dominated by $I_{K,n}$, the input conductance decreased by about 1 nS. There was a consequent reduction of both the inward and the outward currents in the range of potentials from −110 to −60 mV and a shift of the zero-current potential by 2–3 mV in the hyperpolarized direction in the three cells studied.

DISCUSSION

This preparation allows unequivocal identification of the site of origin of recorded OHCs. In previous studies based on isolated cells, the cell location has been left open to question. The preparation also allows patch recordings from cells which more nearly approximate their condition in the intact cochlea. OHCs, recorded in turns 2–4, exhibited lower leak and input conductances compared with isolated cells of comparable length (Ashmore & Meech, 1986; Ashmore, 1987; Santos-Sacchi & Dilger, 1988; Housley & Ashmore, 1992). The significantly more hyperpolarized zero-current potentials found here are also closer to those found by recording microelectrodes *in vivo*, which are typically between −70 and −75 mV (Dallos, 1985). The recordings also allow estimates for the conductances present at such physiological resting potentials.

Each recording site (Fig. 5) can be associated both with a cell length and, on the basis of published cochlear maps, with a best tuning frequency. The cell lengths in the outermost rows of cells at each position are 73 μm (turn 4), 50 μm (turn 3) and 30 μm (turn 2) (Pujol *et al.* 1992). The recording positions reported here correspond to auditory nerve fibres with centre frequencies of approximately 500 Hz (turn 4), 2·2 kHz (turn 3) and 7 kHz (turn 2) based on a map compiled from fibre recording and mechanical measurements (Greenwood, 1990). It is thus possible, using the data in Table 1, to compute the OHC membrane time constant at each of these positions at near physiological membrane potentials as 11·0 ms (turn 4), 3·0 ms (turn 3) and 0·33 ms (turn 2). The equivalent corner frequencies of the low-pass filter represented by the membrane time constants are thus 14, 53 and 480 Hz, respectively, or 0·028, 0·024 and 0·068 of the respective best frequency for that cochlear site. These frequencies, which we consider more representative of the true *in vivo* value, are significantly lower than those previously reported (Housley & Ashmore, 1992). The discrepancy is readily explained as a consequence of the lower leakage conductance applying to recording conditions *in situ*, which allowed an improved estimate of cell input resistance.

The effect of membrane filtering on receptor potentials is thus significant in all cochlear turns. It implies that at the appropriate best frequency, i.e. at the peak of the travelling wave, most of the current passing through the transducer will pass through the membrane capacitance. Some of the implications for models of cochlear tuning have begun to find their way into theoretical models (Dallos & Evans, 1995) and in both linear and non-linear cases (Mammano & Nobili, 1993; Nobili & Mammano, 1996).

Finally, the progressive enhancement in the more basal turns of the current termed $I_{K,n}$ is a means of increasing the input conductance near −70 mV while maintaining the largest driving force for K^+ ions across the apical membrane. Figure 1 shows that $I_{K,n}$ determines the properties of the cell membrane at physiological resting potentials, whereas I_K will only affect the receptor potential if the membrane depolarizes above −40 mV. In most cases, therefore, I_K would be expected to be physiologically 'silent'.

Non-selective currents in outer hair cells

The non-selective current *in situ* amounts to up to 20% of the resting conductance at −70 mV of OHCs in this preparation (Table 1). The leak conductances (Table 1, column 6), measured at −110 mV, were 2·2 nS (turn 4), 2·9 nS (turn 3) and 5·2 nS (turn 2). In isolated cells it can be considerably larger (Housley & Ashmore, 1992). There are results that show OHCs express non-selective currents which are activated by intracellular calcium (Van den Abeele, Tran Ba Huy & Teulon, 1994; Jagger & Ashmore, 1995) as well as by external ATP (Nakagawa, Kakehata, Yamamoto, Akaike, Komune & Uemura, 1991; Housley *et al.* 1992). In the latter case the current activated by extracellular ATP is considerably larger in shorter cells (Housley *et al.* 1995), which suggests that background non-selective currents may be larger in the more basal cochlear turns. There is one further qualification to this conclusion: the main difference between hair cells in this preparation and those found in the intact cochlea, is that the apical surface of the cells in this preparation, where the transducer is located, is not bathed in endolymph (30 μM Ca^{2+}) but in artificial perilymph (1 mM Ca^{2+}). This would lead to an elevation of resting $[Ca^{2+}]_i$ in the cells relative to *in vivo* values. Models of hair cell adaptation which depend on a myosin-dependent motor in the link between stereocilial displacement and mechano-electrical transduction channels (Hudspeth & Gillespie, 1994) imply that the link would be under less tension in the presence (as here) of millimolar Ca^{2+} and therefore a smaller fraction of the transducer channels would remain open. Nevertheless, the simplest explanation for the results of experiments illustrated in Fig. 4, where removal of $[Ca^{2+}]_i$ decreases both K^+ currents, is that elevated $[Ca^{2+}]_i$ increases the activation of $I_{K,n}$, as previously proposed (Housley & Ashmore, 1992).

The above results indicate that two different potassium currents can account for the current–voltage relations *in situ* (Mammano *et al.* 1995). A current, $I_{K,n}$, with properties similar to those of the main conductance active at rest in isolated cells (Housley & Ashmore, 1992) appears to be responsible for most of the cell properties near resting

potential. The implication of the present data, therefore, is that molecular markers for the underlying channel would show a differential expression (relative to other K^+ channels) along the length of the cochlea.

The outward potassium current, I_K, kinetically resembles the currents described in isolated mature OHCs (Santos-Sacchi & Dilger, 1988; Housley & Ashmore, 1992). Its block by 4-AP but partial reduction by TEA distinguish it from several classical calcium-activated potassium channels. Indeed, the chord conductance in nominally zero external Ca^{2+} decreased less between −40 and 0 mV, the steepest activation range for I_K, than near the zero-current potential (Fig. 4). This suggests that $[Ca^{2+}]_i$ has less effect on I_K than on $I_{K,n}$ *in situ*.

Art, J. J. & Fettiplace, R. (1987). Variation of membrane properties in hair cell isolated from the turtle cochlea. *Journal of Physiology* **385**, 207–242.

Ashmore, J. F. (1987). A fast motile response in guinea-pig outer hair cells: the cellular basis of the cochlear amplifier. *Journal of Physiology* **388**, 323–347.

Ashmore, J. F. (1989). Transducer motor coupling in outer hair cells. In *Cochlear Mechanism: Structure, Function and Models*, ed. Wilson, J. P. & Kemp, D. T., pp. 107–113. Plenum Press, New York.

Ashmore, J. F. & Meech, R. W. (1986). Ionic basis of membrane potential in outer hair cells of the guinea-pig cochlea. *Nature* **322**, 368–371.

Dallos, P. (1985). Response characteristics of mammalian cochlear hair cells. *Journal of Neuroscience* **5**, 1591–1608.

Dallos, P. & Evans, B. N. (1995). High frequency motility of outer hair cells and the cochlear amplifier. *Science* **267**, 2006–2009.

Dennis, J. E. Jr & Woods, D. J. (1987). Optimization on microcomputers – the Nelder–Mead simplex algorithm. In *New Computing Environments: Microcomputers in Large-scale Computing*, ed. Wouk, A., pp. 123–129. SIAM Publishing, Philadelphia.

Greenwood, D. D. (1990). A cochlear frequency–position function for several species – 29 years later. *Journal of the Acoustical Society of America* **87**, 2592–2605.

Housley, G. D. & Ashmore, J. F. (1992). Ionic currents of outer hair cells isolated from the guinea-pig cochlea. *Journal of Physiology* **448**, 73–98.

Housley, G. D., Connor, B. J. & Raybould, N. P. (1995). Purinergic modulation of outer hair cell electromotility. In *Active Hearing*, ed. Flock, A., Ottoson, D. & Ulfendahl, M., pp. 113–125. Elsevier Science, Oxford.

Hudspeth, A. J. & Gillespie, P. G. (1994). Pulling strings to tune transduction: Adaptation by hair cells. *Neuron* **12**, 1–9.

Jagger, D. J. & Ashmore, J. F. (1995). Effect of intracellular calcium release on ionic currents in outer hair cells isolated from the guinea-pig cochlea. *Journal of Physiology* **489.P**, 48*P*.

Mammano, F. & Ashmore, J. F. (1993). Reverse transduction measured in the isolated cochlea by laser Michelson interferometry. *Nature* **365**, 838–841.

Mammano, F. & Ashmore, J. F. (1995). Differential expression of outer hair cell potassium currents in the apical turns of the isolated cochlea of the guinea-pig. *Journal of Physiology* **485.P**, 30*P*.

Mammano, F., Kros, C. J. & Ashmore, J. F. (1995). Patch clamped responses from outer hair cells in the intact adult organ of Corti. *Pflügers Archiv* **430**, 745–750.

Mammano, F. & Nobili, R. (1993). Biophysics of the cochlea. Linear approximation. *Journal of the Acoustical Society of America* **93**, 3320–3332.

Murrow, B. W. (1994). Position-dependent expression of potassium currents by chick cochlear hair cells. *Journal of Physiology* **480**, 247–259.

Nakagawa, T., Kakehata, S., Akaike, N., Komune, S., Takasaka, T. & Uemura, T. (1991). Calcium channel in isolated outer hair cells of guinea pig cochlea. *Neuroscience Letters* **125**, 81–84.

Nakagawa, T., Kakehata, S., Yamamoto, T., Akaike, N., Komune, S. & Uemura, T. (1994). Ionic properties of $I_{K,n}$ in outer hair cells of the guinea pig cochlea. *Brain Research* **661**, 293–297.

Nobili, R. & Mammano, F. (1996). Biophysics of the cochlea. II. Steady-state non linear phenomena. *Journal of the Acoustical Society of America* **99**, 2244–2255.

Press, W. H., Flannery, B. P., Teukolsky, S. A. & Vetterling, W. T. (1988). *Numerical Recipes in C*, pp. 528–540. Cambridge University Press, Cambridge, UK.

Pujol, R., Lenoir, M., Ladrech, S., Trebillac, F. & Rebillard, G. (1992). Correlation between the length of outer hair cells and the frequency coding of the cochlea. In *Auditory Physiology and Perception*, ed. Cazals, Y., Demeny, L. & Horner, K., pp. 45–52. Pergamon Press, Oxford.

Santos-Sacchi, J. (1991). Reversible inhibition of voltage-dependent outer hair cell motility and capacitance. *Journal of Neuroscience* **11**, 3096–3110.

Santos-Sacchi, J. & Dilger, J. P. (1988). Whole-cell currents and mechanical responses of isolated outer hair cells. *Hearing Research* **35**, 143–150.

Spoendlin, H. (1978). The afferent innervation of the cochlea. In *Evoked Electrical Activity in the Auditory Nervous System*, ed. Naunton, R. F. & Fernandez, C., pp. 21–39. Academic Press, London.

Van den Abbeele, T., Tran Ba Huy, P. & Teulon, J. (1994). A calcium-activated non-selective cation channel in the basolateral membrane of outer hair cells of the guinea-pig cochlea. *Pflügers Archiv* **417**, 56–63.

Vôldrich, L. (1983). Experimental and topographic morphology in cochlear mechanics. In *Mechanics of Hearing*, ed. de Boer, E. & Viergever, M. A., pp. 163–167. Martinus Nijhoff, Amsterdam.

Acknowledgements

This work was supported by The Wellcome Trust and the EC (Basic Research Action, SSS 6961). Dr C. J. Kros participated in some of the early experiments on third turn outer hair cells.

Author's present address

F. Mammano: Biophysics Laboratory, International School for Advanced Studies, Via Beirut 2-4, 34014 Trieste, Italy.

Authors' email address

J. F. Ashmore: j.ashmore@ucl.ac.uk

F. Mammano: mammano@sissa.it

Received 23 January 1996; accepted 23 July 1996.